

Deterministically Charged Quantum Dots in Photonic Crystal Nanoresonators for Efficient Spin-Photon Interfaces

Konstantinos G. Lagoudakis^a, Kevin Fischer^a, Tomas Sarmiento^a, Arka Majumdar^b,
Armand Rundquist^a, Jesse Lu^a, Michal Bajcsy^a & Jelena Vučković^a

^a*E. L. Ginzton Laboratory, Stanford University, Stanford CA 94305, USA*

^b*Department of Physics, University of California, Berkeley, CA 94720, USA*

We demonstrate a novel method for deterministic charging of InAs quantum dots embedded in photonic crystal nanoresonators using a unique vertical *p-n-i-n* junction within the photonic crystal membrane. Charging is confirmed by the observation of Zeeman splitting for magnetic fields applied in the Voigt configuration. Spectrally resolved photoluminescence measurements are complemented by polarization resolved studies that show the precise structure of the Zeeman quadruplet. Integration of quantum dots in nanoresonators strongly enhances far-field collection efficiency and paves the way for the exploitation of enhanced spin-photon interactions for fabrication of efficient quantum nodes in a scalable solid state platform.

Systems involving single quantum emitters interacting with photons are not only interesting in the context of quantum optics and cavity quantum electrodynamics but have been shown to be excellent candidates for quantum information processing and communications. Along these lines, a requirement of utmost importance is efficient interfacing of flying and stationary qubits. Some of the most promising platforms for the realization of such interfaces, are superconducting circuits^{1,2}, trapped ions and ion chains^{3,4}, nitrogen vacancies in diamond^{5,6}, and atoms in cavities^{7,8}. The platform of photonic crystals with embedded quantum dots (QDs) is another very promising system where efficient interfacing of flying and stationary qubits can be implemented for the creation of scalable quantum networks and quantum information processing⁹.

Although neutral QDs could be used as stationary qubits, they suffer from relatively short coherence times¹⁰ on the order of a nanosecond. On the other hand, the ground states of quantum dots containing an additional electron are characterized by coherence times that are many orders of magnitude longer¹¹ (100s of μsec) and therefore are much better suited for use as qubits. Furthermore, the optical addressability of these states allows for ultrafast control.

Probabilistically charged quantum dots in bulk materials have been successfully used for qubit initialization and manipulation¹², but the low charging efficiencies and the probabilistic nature of the charging of the QDs present serious limitations to this approach. Several methods have been proposed and implemented for deterministic charging of QDs in order to eliminate these issues: Schottky junctions¹³ or lateral¹⁴ and more commonly vertical *p-i-n* junctions¹⁵⁻¹⁷.

Integration of junction-embedded photonic crystal nanoresonators with quantum dots allows for significant efficiency improvements. In addition to the enhancement of far-field collection efficiency, the ability to confine light to

extremely small mode volumes (of the order $(\lambda/n)^3$) greatly enhances the interaction between photons and quantum dots.

Several geometries have been proposed for interfacing charged QD spin to photons by means of either orthogonally polarized degenerate H1 cavities¹⁸ or linearly polarized defect L3 cavities. Very recently, experimental efforts based on nearly resonant L3 nanoresonators have shown exciting results on spin initialization and manipulation¹⁷. Since the metallic films required for Schottky junctions drastically reduce nanoresonator quality factor, *p-i-n* junctions are better suited for use with the photonic crystal platform. Yet, while *p-i-n* structures have been very successful for deterministic charging, several issues need to be addressed, most notably the relatively high bias involved for charging the dots and the difficulty in imposing the sign of the charging.

Here we investigate a novel structure for deterministic charging of QDs in photonic crystal nanoresonators, based on a vertical *p-n-i-n* geometry that has reduced built-in bias while allowing for negative charging of the QDs on demand. We perform a detailed magneto-spectroscopic study of QDs in close resonance to photonic crystal nanoresonators and demonstrate charging by the application of a strong magnetic field in the Voigt configuration that results in the characteristic quadruplet Zeeman splitting of charged dots¹⁹. The sample that was used in this study consists of a 164 nm GaAs membrane with a *p-n-i-n* doping profile (Fig. 1(a)), containing InAs QDs in the center of the intrinsic region. An 873 nm thick $\text{Al}_{0.8}\text{Ga}_{0.2}\text{As}$ sacrificial layer allows release of the membrane when undercut. A distributed Bragg reflector consisting of 5 alternating GaAs- $\text{Al}_{0.8}\text{Ga}_{0.2}\text{As}$ quarter-wavelength layers was grown underneath the sacrificial layer in order to enhance collection efficiency. Gold pads were deposited on both sides of the sample, as shown in Fig. 1(b), in order to electrically contact the device. Electron beam lithography followed by inductively coupled plasma etching was used to pattern the arrays of nanoresonators. A scanning

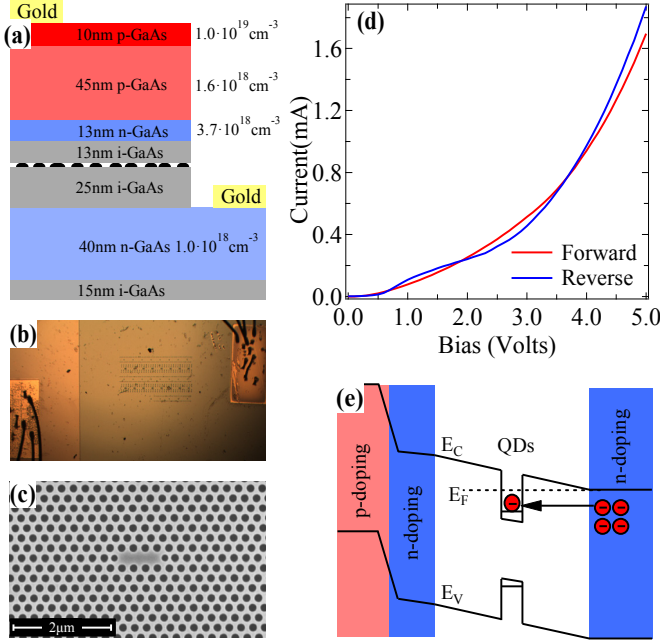


FIG. 1: (a) Photonic crystal membrane composition and doping profile. The quantum dots are depicted as the black domes at the center of the membrane. (b) Low magnification optical microscope image of the sample. The wire bonded contact pads are seen at the two sides while an array of nanocavities can be seen between the pads. The lightly shaded region around the left pad corresponds to the etched part that exposes the bottom n -doped layer. (c) SEM image of an L3 cavity. (d) I-V curve of the sample at cryogenic temperature. (e) Schematic band diagram of the p - n - i - n junction. E_V is the valence and E_C the conduction band and E_F corresponds to the Fermi level. Layer thicknesses are not up to scale.

electron microscope (SEM) image of an L3 cavity is shown in Fig. 1(c). The lower n -doped region was exposed using a

Piranha wet etch, allowing for both the p and n layers of the junction to be contacted⁹.

The sample was held at approximately 10 K on the cold finger of a continuous helium flow cryostat whose superconducting magnet supports a maximum field of $B_{\text{max}}=5\text{T}$. In order to apply a magnetic field in the Voigt configuration, the sample was oriented with its growth direction perpendicular to the magnetic field lines. A special holder with a mirror oriented at 45° above the sample allows for easy optical access of the sample surface. QD luminescence was collected with a long working distance microscope objective with 0.5NA followed by a standard confocal microscopy setup with polarization resolution. A polarization maintaining 10:90 beam splitter was used to minimize losses of the collected luminescence. QD luminescence was generated by pumping with an above band cw laser at 780 nm. The photoluminescence spectra were recorded at the output of a 0.75 m long monochromator with a $\sim 45 \mu\text{eV}$ resolution. In order to study the junction's electrical response, an ultra-stable power supply was used to scan the applied voltage across the junction. A typical I-V curve of the sample studied here is provided in Fig. 1(d) showing diode-like characteristics. Its non-ideal behavior comes from residual resistive channels created through fabrication imperfections such as spurious gold deposition on the sample edges, degradation of ohmic contacts due to oxidation, and possible gold diffusion through the membrane during wire-bonding. These resistive channels also lead to an overestimate of the electrical bias voltage applied across the junction.

The p - n - i - n structure is designed to favor negative charging of the QDs by blocking hole injection at the p - n junction. The doping and thicknesses of these p and n layers are such that the energy bands in the intrinsic region are slightly tilted for zero forward bias, as can be seen in the schematic representation of Fig. 1(e). Application of a forward bias pushes the excess carriers of the bottom n -doped region further in the intrinsic region where the QDs are

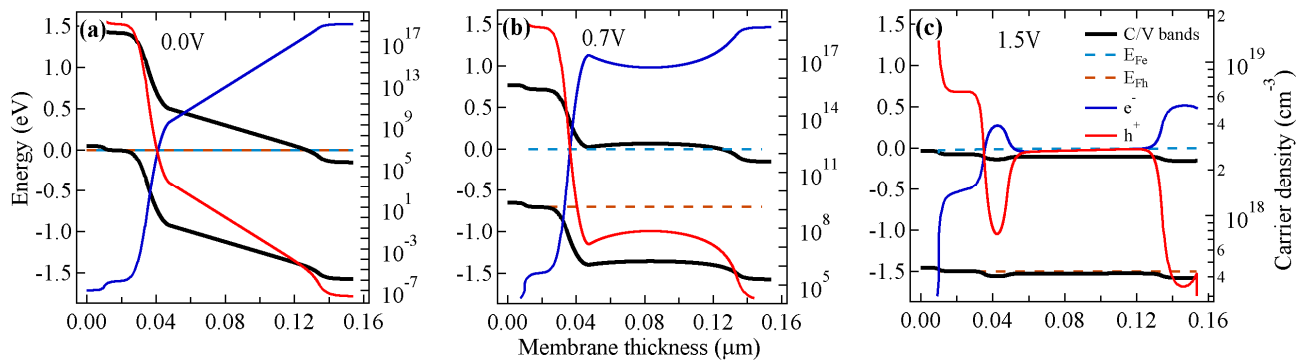


FIG. 2: Simulated band structure (black lines), quasi-Fermi levels for electrons (orange) and for holes (green) and carrier densities (red for holes and blue for electrons) along the growth direction for three different forward biases (a) 0 volts, (b) 0.7 volts and (c) 1.2 volts. The carrier densities are plotted against the right-hand axis whereas the energies of conduction and valence bands and the quasi-Fermi levels are plotted against the left-hand axis. The inbuilt field that bends the bands at zero bias is counterbalanced when a forward bias is applied, resulting in a flattening of the bands. The high electron density at the central region (80nm beneath the membrane surface) where the quantum dots are situated ensures negative charging of the quantum dots. For simulations, we employ Sentaurus solver.

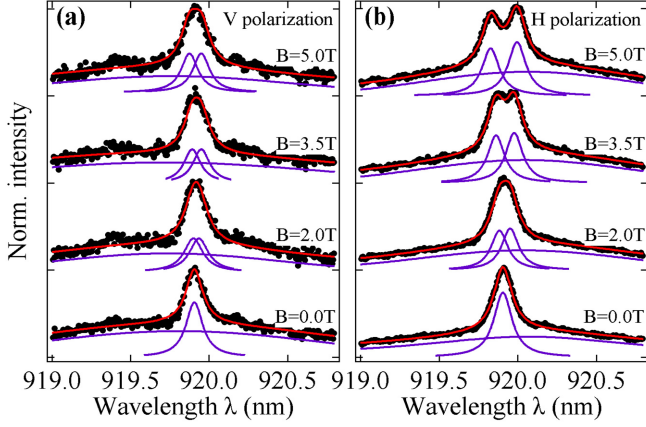


FIG. 3: Multi-fits of the spectral response of a typical QD for four values of the applied magnetic field for vertical (a) and horizontal (b) polarizations. Black points correspond to the raw spectra and the red solid line is the fitted lineshape. Violet solid lines are the individual peaks that were fitted and the sum of those results in the overall fit.

located, favoring injection of electrons into the QDs and therefore favoring negative charging. In addition, the application of a forward bias counter balances the effect of the built-in field, resulting in a flattening of the bands as shown in Fig. 2(b) and 2(c).

For low forward biases carriers that are generated optically by the above band excitation in the vicinity of the QDs are separated in the intrinsic region of the junction because of the inbuilt field and the spatially mismatched wavefunctions of electrons and holes within the quantum dots. The cumulative effects of charge separation and spatial mismatch lead to weak photoluminescence intensity. As the conduction and valence bands flatten out at higher forward bias we observed an increase in the photoluminescence intensity as well as a gradual shift of the QD towards higher energies as a result of the quantum confined Stark effect.

Although the structure is designed to favor formation of negatively charged trions within the QDs and potential charging evidence was observed at zero magnetic field in the form of spectral jumps, conclusive evidence of charging can only be observed after the application of a magnetic field in the Voigt configuration. Application of the magnetic field in this particular configuration results in four optically active transitions in the spectrum between spin-mixed electron and trion state. The Zeeman splitting of the ground state is determined solely by the g -factor of the electron. On the other hand, since the electron pair of the lowest energy trions share the same orbital, they are in a spinless singlet state due to the Pauli Exclusion Principle and therefore only the g -factor of the holes contribute to the Zeeman splitting of the trion states. The selection rules that govern the quadruplet impose orthogonal linear polarization between the two outer and two inner transitions¹⁹. Contrary to this characteristic behavior of charged dots, neutral quantum dots do not show splitting for

the magnetic fields achievable with our superconducting magnet. Thus, spectroscopic characterization with polarization resolution under magnetic field is used to eliminate ambiguity in the deterministic charging capacity of our device. To perform this experiment, the device was driven at a low forward bias $V_f=1.2V$ chosen for high QD photoluminescence intensity and high probability of negative QD charging.

Upon application of the magnetic field, the spectroscopic signature of the QD radically changes showing significant broadening at low fields that develops into a full quadruplet structure at high magnetic field. The locations of the individual peaks were extracted from the spectra by decomposing the overall spectral response into Lorentzian peaks by least squares regression. The individual fitted peaks along with the overall fit and raw data is shown in Fig. 3 for the two polarizations. The linewidths of the individual QD transitions are expected to be close to that of the zero applied field transition linewidth, here being of the order of 0.1 nm. This width is a convolution of the actual QD lineshape with the response function of the monochromator, which is highly dependent on the monochromator slit width and grating type. The peak locations of the multi-fits for all the magnetic fields are shown in Fig. 4. The trend of the splitting is given by the sum of the linear Zeeman splitting, a global quadratic shift related to the diamagnetic shift and any temperature fluctuations while changing the magnetic field. The raw data peak locations are shown in Fig. 4(a) while the actual linear Zeeman splitting after removal of the diamagnetic shift is shown in Fig. 4(b).

The slope of the outer and inner transitions provide the sum and difference of the g Landé factors of electrons and holes from which we extracted $g_e=0.25\pm0.05$ and $g_h=0.60\pm0.01$, in agreement with recent literature²⁰. Contrary to what was recently reported on the dependence of the g factors of electrons and holes as a function of the applied bias in a $p-i-n$ structure²⁰, here we do not observe a similar effect. The splitting and polarization properties remain the same for a wide range of applied biases. The demonstration of the quadruplet spectral structure for a magnetic field in the Voigt

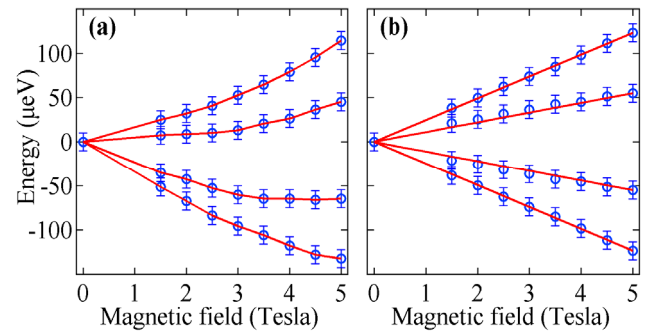


FIG. 4: (a) Locations of the fitted peaks from the raw data. The diamagnetic shift along with any temperature fluctuations bend the splitting lines. (b) Pure Zeeman splitting after removal of the diamagnetic shift.

configuration demonstrates conclusively that QDs in this structure are charged upon application of a small forward bias.

The device presented here utilizes a novel structure for deterministic charging of QDs in close resonance to photonic crystal nanoresonators. Compared to the usual p - i - n membrane doping structure, the p - n - i - n profile used here acts to flatten the bands at the operating bias resulting in high negative charging probability. Simultaneously, it keeps the positive excess carrier density low in the vicinity of the QD, while the n region on the other end of the structure provides the high electron density to allow for deterministic negative charging of the QDs. The charging is demonstrated conclusively by the application a magnetic field in the Voigt configuration observation of a quadruplet splitting of the QD

resonance. Inversing the doping profile should allow for positive charging of the QDs on demand, which could be of future interest²¹. Future investigations will employ resonant excitation for the investigation of the charged QD linewidth and the general suitability of this device for spin photon interfaces.

The authors acknowledge financial support provided by the Air Force Office of Scientific Research, MURI Center for Multi-functional light-matter interfaces based on atoms and solids. K.G.L. acknowledges support from the Swiss National Science Foundation. K.F. acknowledges support from the Stanford Graduate Fellowship.

¹ A. Wallraff, D.I. Schuster, A. Blais, L. Frunzio, R.-S. Huang, J. Majer, S. Kumar, S.M. Girvin, and R.J. Schoelkopf, *Nature* **431**, 162 (2004).

² J.M. Fink, M. Göppl, M. Baur, R. Bianchetti, P.J. Leek, A. Blais, and A. Wallraff, *Nature* **454**, 315 (2008).

³ M. Keller, B. Lange, K. Hayasaka, W. Lange, and H. Walther, *Nature* **431**, 1075 (2004).

⁴ T. Monz, P. Schindler, J.T. Barreiro, M. Chwalla, D. Nigg, W.A. Coish, M. Harlander, W. Hänsel, M. Hennrich, and R. Blatt, *Phys. Rev. Lett.* **106**, 130506 (2011).

⁵ E. Togan, Y. Chu, A.S. Trifonov, L. Jiang, J. Maze, L. Childress, M.V.G. Dutt, A.S. Sørensen, P.R. Hemmer, A.S. Zibrov, and M.D. Lukin, *Nature* **466**, 730 (2010).

⁶ M.V.G. Dutt, L. Childress, L. Jiang, E. Togan, J. Maze, F. Jelezko, A.S. Zibrov, P.R. Hemmer, and M.D. Lukin, *Science* **316**, 1312 (2007).

⁷ J. McKeever, A. Boca, A.D. Boozer, J.R. Buck, and H.J. Kimble, *Nature* **425**, 268 (2003).

⁸ A. Kuhn, M. Hennrich, and G. Rempe, *Phys. Rev. Lett.* **89**, 067901 (2002).

⁹ A. Faraon, A. Majumdar, D. Englund, E. Kim, M. Bajcsy, and J. Vučković, *New J. Phys.* **13**, 055025 (2011).

¹⁰ P. Borri, W. Langbein, S. Schneider, U. Woggon, R.L. Sellin, D. Ouyang, and D. Bimberg, *Phys. Rev. Lett.* **87**, 157401 (2001).

¹¹ M. Kroutvar, Y. Ducommun, D. Heiss, M. Bichler, D. Schuh, G. Abstreiter, and J.J. Finley, *Nature* **432**, 81 (2004).

¹² D. Press, T.D. Ladd, B. Zhang, and Y. Yamamoto, *Nature* **456**, 218 (2008).

¹³ M. Ediger, P.A. Dalgarno, J.M. Smith, B.D. Gerardot, R.J. Warburton, K. Karrai, and P.M. Petroff, *Applied Physics Letters* **86**, 211909 (2005).

¹⁴ B. Ellis, T. Sarmiento, M. Mayer, B. Zhang, J. Harris, E. Haller, and J. Vuckovic, *Appl. Phys. Lett.* **96**, 181103 (2010).

¹⁵ D. Pinotsi, P. Fallahi, J. Miguel-Sanchez, and A. Imamoglu, *IEEE J.Q.E.* **47**, 1371 (2011).

¹⁶ D. Pinotsi, J.M. Sanchez, P. Fallahi, A. Badolato, and A. Imamoglu, *Photonics and Nanostructures - Fundamentals and Applications* **10**, 256 (2012).

¹⁷ S.G. Carter, T.M. Sweeney, M. Kim, C.S. Kim, D. Solenov, S.E. Economou, T.L. Reinecke, L. Yang, A.S. Bracker, and D. Gammon, *Nat Photon* **7**, 329 (2013).

¹⁸ A. Majumdar, P. Kaer, M. Bajcsy, E.D. Kim, K.G. Lagoudakis, A. Rundquist, and J. Vučković, *Phys. Rev. Lett.* **111**, 027402 (2013).

¹⁹ M. Bayer, G. Ortner, O. Stern, A. Kuther, A.A. Gorbunov, A. Forchel, P. Hawrylak, S. Fafard, K. Hinzer, T.L. Reinecke, S.N. Walck, J.P. Reithmaier, F. Kloppe, and F. Schäfer, *Phys. Rev. B* **65**, 195315 (2002).

²⁰ A.J. Bennett, M.A. Pooley, Y. Cao, N. Sköld, I. Farrer, D.A. Ritchie, and A.J. Shields, *Nat Commun* **4**, 1522 (2013).

²¹ B.D. Gerardot, D. Brunner, P.A. Dalgarno, P. Ohberg, S. Seidl, M. Kroner, K. Karrai, N.G. Stoltz, P.M. Petroff, and R.J. Warburton, *Nature* **451**, 441 (2008).